Journal of Power Sources 195 (2010) 4278–4284

Contents lists available at ScienceDirect

Journal of Power Sources

journal homepage: www.elsevier.com/locate/jpowsour

Re-examining the effect of ZnO on nanosized 5 V $LiNi_{0.5}Mn_{1.5}O_4$ spinel: An effective procedure for enhancing its rate capability at room and high temperatures

J.C. Arrebola, A. Caballero, L. Hernán, J. Morales*

Departamento de Química Inorgánica e Ingeniería Química, Campus de Rabanales, Edificio Marie Curie, Universidad de Córdoba, 14071 Córdoba, Spain

ARTICLE INFO

Article history:
Received 9 September 2009
Received in revised form
21 December 2009
Accepted 3 January 2010
Available online 11 January 2010

Keywords:
Nanospinel
Coating
Zinc oxide
High voltage
Lithium batteries

ABSTRACT

Based on the known effectiveness of ZnO as a hypothetical coating, its ability to expand the rate capability of nanosized $LiNi_{0.5}Mn_{1.5}O_4$ was examined. The additive was characterized by X-ray photoelectron spectroscopy (XPS) analysis. The intensity of the 2p peak for Zn in the XPS concentration depth profiles remained unchanged over a long sputtering period; therefore, rather than forming a coating layer over the spinel particles, as commonly described in the literature, ZnO seemingly deposits as uniformly dispersed nanoparticles in the bulk material. TEM images were consistent with this alternative model for explaining where the oxide is located. ZnO-treated spinel cycled at low rates (*C*/4) at room temperature was found to exhibit an increase in delivered capacity (more than a 10%) with good capacity retention. The increase was less marked at high cycling rates (8*C*). Cells cycled at 50 °C exhibited similarly improved properties; however, the increase in capacity at low cycling rates was somewhat lower. These changes are explained in the light of the results obtained by treating the spinel with HF at room temperature: ZnO clearly hindered dissolution of the spinel. In fact, ZnO partially protects the spinel from the attack of HF traces in $LiPF_6$ based electrolyte during prolonged contact between the two. This protective effect, however, is insubstantial at high charge/discharge rates, where contact between the spinel and electrolyte is shorter.

1. Introduction

The gradual development of portable technology has aroused a growing interest in portable power systems. In this context, batteries (especially of the lithium-ion type [1]) emerged as an interesting choice a few years ago. For such batteries to meet the energy requirements, they must be able to deliver a high power; afford cycling at high current densities in order to ensure charging within a short time; and possess a high rate capability. The spinel $LiNi_{0.5}Mn_{1.5}O_4$ meets some of these requirements. Thus, it combines a high capacity (theoretical value 148 mAh g^{-1}) and a high potential (4.8 V vs. Li) [2–4]. In the form of highly crystalline nanometric (<100 nm) particles, this spinel provides an outstanding electrochemical response at high charge/discharge rates and exhibits a high rate capability [5–9]. However, nanometric particles have a serious drawback in their increased reactivity compared with microparticles. Thus, contact with the electrolyte can lead to partial Ni and/or Mn dissolution from them, especially when the cell operates at low rates and contact between the active material and electrolyte is quite prolonged.

One other major requisite for lithium-ion batteries is retention of good performance at high temperatures. Under these conditions, the specific capacity can undergo a severe drop by effect of the substantial presence of side reactions such as electrolyte decomposition by water traces [10] $LiPF_6 + H_2O \rightarrow POF_3 + LiF + 2HF$. The hydrofluoric acid formed can attack active materials such as Li–Ni–Mn based spinels and detract from cell performance as a result. The combination of high temperatures and a reduced particle size increases the spinel instability in the electrolyte, thus facilitating its dissolution. One way of reducing the spinel decomposition and hence, the adverse effect of the electrolyte, is by coating the active particles with an inert matrix acting as protective layer against the attack by HF. The additives used to improve the electrochemical behavior of $LiNi_{0.5}Mn_{1.5}O_4$ range from noble metals such as Ag [11] and Au [12] to quite stable compounds such as ZnO [13–16]. These materials seemingly act differently and their exact mechanism remains unclear in some cases. Such is the case with ZnO, the action of which has been explained in various terms even by the same authors. Thus, Sun et al. [15] have suggested inhibition of the formation of an undefined graphitic phase over the surface of the active material as the origin of the improved elec-

* Corresponding author. Tel.: +34 957 218620; fax: +34 957 218621.
E-mail address: iq1mopaj@uco.es (J. Morales).

0378-7753/$ – see front matter © 2010 Elsevier B.V. All rights reserved.
doi:10.1016/j.jpowsour.2010.01.004

trochemical response. However, the group led by Sun et al. [13,14] have also ascribed the effect of the oxide to its ability to react with HF thanks to its amphoteric character. In this way, the spinel is protected from attack by the acid. The outcome is improved cell performance at both ambient temperature and higher levels.

Based on the effective action of ZnO as a protective agent, in this work we assessed its efficiency in enhancing the rate capability of nanosized $LiNi_{0.5}Mn_{1.5}O_4$ over a wide range of charge/discharge currents (*C*/4–8*C*), a relevant property the study of which is indeed crucial with a view to assess the potential uses of electrode materials. The main weakness of nanometric particles in this context (viz. their poor performance at low cycling rates) was overcome by effect of the protective action of ZnO, which is particularly effective at low rates, the nanoparticles retaining their good performance at high rates. We have re-examined the protective effect of ZnO by using a more direct method than that of Sun et al. [15] and based on how the oxide reduces the solubility of the spinel by effect of the release of HF. This test, which is better suited to the actual process and subject to very small errors by effect of its using such a powerful analytical technique as Inductively Coupled Plasma spectroscopy, is more accurate in exposing the role played by ZnO. The decreased solubility of the ZnO-treated spinel provides direct evidence of the beneficial effect of this oxide on the spinel stability under the operating conditions used.

The low concentration of ZnO precludes its detection by X-ray diffraction (XRD) [13–16]. Also, other characterization techniques such as energy dispersive by X-ray (EDAX) analysis allow the metal to be identified but provide no information about the structural characteristics of the compound. In this work, we used X-ray photoelectron spectroscopy (XPS) in combination with depth profile analysis as an effective integral tool to establish the composition of the first few outermost layers of the material and also to derive information about the distribution of ZnO and its location relative to the spinel nanoparticles.

2. Experimental

A spinel of nominal stoichiometry $LiNi_{0.5}Mn_{1.5}O_4$ was obtained by using a polymer-assisted method described elsewhere [8] that yields highly crystalline nanosized particles of ca. 80 nm. The coating was obtained by dispersing $Zn(CH_3COO)_2{\cdot}2H_2O$ in ethanol and added to the spinel in a 99:1 ($LiNi_{0.5}Mn_{1.5}O_4$/ZnO) mole ratio. After 15 min shaking, the solvent was evapored by raising the temperature and the solid calcined at 450 °C for 5 h to discompose the organic residue. The two samples thus obtained were treated with an aqueous solution of HF (40%) (supplied by Sigma–Aldrich) at room temperature under continuous stirring for one week. Unreacted particles were separated by centrifugation and the liquid phase stored for subsequent determination of Ni and Mn by ICP on a Fisons ARL-3410 instrument.

X-ray diffraction (XRD) patterns were recorded on a Siemens D5000 X-ray diffractometer using non-monochromatic Cu Kα radiation and a graphite monochromator for the diffracted beam. The scanning conditions for structural refinement were 15–80° (2θ), a 0.03° step size and 12 s per step. XPS spectra were obtained on a Physical Electronics PHI 5700 spectrometer using non-monochromatic Mg Kα radiation (300 W, 15 kV, 1253.6 eV) and a multi-channel detector. Spectra for the disc samples were recorded in the constant pass energy mode at 29.35 eV, using a 720 μm diam analysis area. Binding energy values were referred to the C 1 s peak (284.8 eV) from the adventitious contamination layer during data processing of the XPS spectra. The CA PHI ACCESS ESCA-V6.0 F software package was used for data acquisition and processing. An Ar^+ ion beam of 4 kV was used for depth profiling and compositions were determined from the integrated intensities of the XPS spectra.

Electrochemical measurements were made on R2032 coin-type cells supplied by Hohsen. The cathode was made from a mixture containing 6 mg of spinel and 1.5 mg of carbon black (super P) that was pressed at 221.5 MPa onto a stainless steel grid (13 mm diameter). No binder was used to prepare the electrode, however. Lithium metal (supplied by Strem) was used as anode and isolated from the cathode by means of a porous propylene film. The electrolyte, supplied by Merck, was 1 M anhydrous $LiPF_6$ in a 1:1 mixture of ethylene carbonate and dimethyl carbonate. Cells were assembled in an M-Braun glove-box. Galvanostatic tests were conducted under different charge/discharge regimes (from *C*/4 to 8*C*, *C* representing 1 Li^+-ion exchanged in 1 h, equivalent to 148 mA g^{-1}). The electrochemical measurements were controlled via a MacPile II potentiostat–galvanostat. All measurements were made at least in duplicate in order to ensure reliability in the electrochemical results.

3. Results and discussion

3.1. Sample characterization

Table 1 shows selected properties of the spinel. As can be seen, it was virtually stoichiometric and contained only a very small excess of Mn relative to Ni. This may have resulted the presence of impurities assigned to either NiO and/or $Li_xNi_{1-x}O$ which amounted to less than 6% as quantified by Rietveld analysis. Fig. 1 shows the XRD patterns for the two samples, $LiNi_{0.5}Mn_{1.5}O_4$ and $LiNi_{0.5}Mn_{1.5}O_4$/ZnO. As can be seen, the presence of ZnO altered the position of none of the diffraction peaks for the spinel. The difference in lattice parameters between the two samples was negligible (8.1824 vs. 8.183 Å), which confirms that ZnO does not diffuse into the spinel structure. Also, no peaks for the coating oxide, ZnO, were detected. This may have been a result of (i) the small amount of ZnO added and/or (ii) its low crystallinity. One interesting finding was that particle size and shape were retained after the addition of ZnO. Also, crystallite size as determined by X-ray broadening analysis was similar for both samples (see Table 1) and the well-defined polyhedral morphology of the nanoparticles was preserved after treatment (see Fig. 2). Retention of particle size and crystallinity was to be expected since

Table 1
Composition, lattice parameters, specific surface area and crystallite size of the bare Li–Ni–Mn–O and treated with ZnO-coated spinels.

Sample	Formula	*a* (Å)	S_{BET} (m^2g^1)	*D* (nm)
$LiNi_{0.5}Mn_{1.5}O_4$	$Li_{1.01}Ni_{0.48}Mn_{1.54}O_4$	8.1824 (7)	15.5	79
$LiNi_{0.5}Mn_{1.5}O_4$/ZnO	–	8.183 (1)	–	71

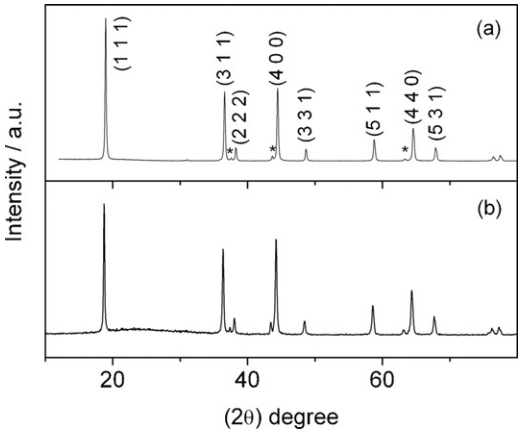

Fig. 1. XRD patterns for (a) the pristine spinel and (b) $LiNi_{0.5}Mn_{1.5}O_4$/ZnO.

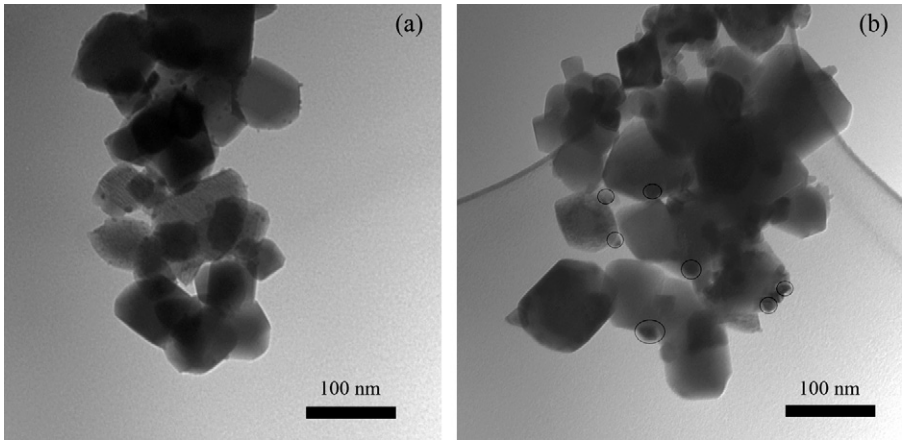

Fig. 2. TEM images for (a) the pristine spinel and (b) $LiNi_{0.5}Mn_{1.5}O_4$/ZnO (ZnO particles are labelled by circles).

the calcining temperature required for ZnO to form was only 450 °C – which is too low for sintering to occur.

Detecting ZnO required the use of the XPS technique. Fig. 3a shows the XPS spectrum for the $LiNi_{0.5}Mn_{1.5}O_4$/ZnO sample in the Zn 2p region. The two peaks at 1021.1 eV and 1044.5 eV can be assigned to $2p_{3/2}$ and $Zn2p_{1/2}$ photoemission, respectively, consistent with those previously reported for ZnO compound [17]. A more accurate characterization of the ZnO–$LiNi_{0.5}Mn_{1.5}O_4$ system was accomplished from XPS depth profiles. Fig. 3b shows the concentrations of the constituent elements of the spinel (the amount of lithium was difficult to determine accurately owing to the very low scattering power of this element to X-Rays) and zinc as a function of the sputtering time. Carbon was the sole element the content in which decreased with etching; after only a few minutes, its concentration fell to 10% the initial value, similarly to carbon black added to the pellet. The carbon removed was essentially adventitious carbon since no peaks for oxygen-bound carbon were observed. Oxygen, manganese and nickel increased in concentration during the first few minutes of etching and then levelled off on prolonged etching. As for the Zn profile, the initial concentration, close to 1%, was consistent with the amount added to the spinel. The amount of Zn was also determined by EDX analysis. The Zn/Mn ratio obtained was 0.010, very close to the stoichiometric value (0.008). The variation of the Zn concentration with the sputtering time exhibited small fluctuations rather than a well-defined trend to disappear on prolonged etching. This shed some light on the location of ZnO. On the assumption of a depth value of 10 nm per min of Ar^+ etching [18], the coating layer thickness should amount to more than one micron, which is even much greater than the spinel particle size. Virtually complete removal of the coating from the surface of the particles by ionic ablation has been reported to occur when the

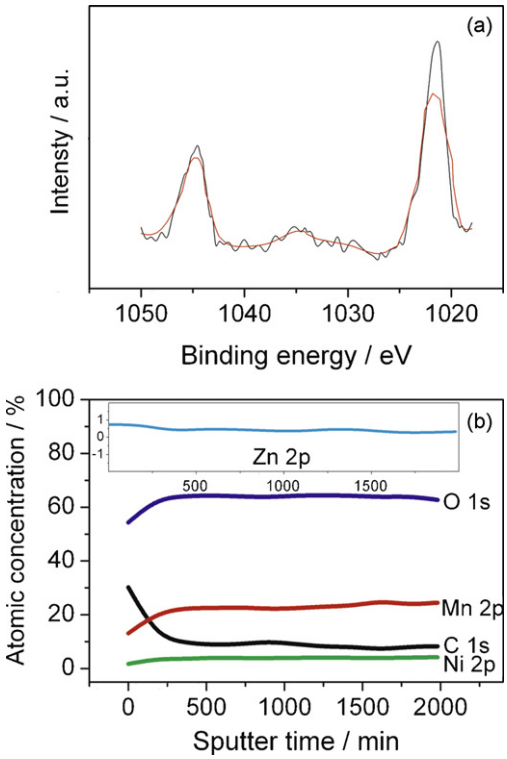

Fig. 3. (a) X-ray photoelectron spectra for the Zn 2p ($LiNi_{0.5}Mn_{1.5}O_4$/ZnO) and (b) XPS depth profile for $LiNi_{0.5}Mn_{1.5}O_4$/ZnO containing 10% carbon black.

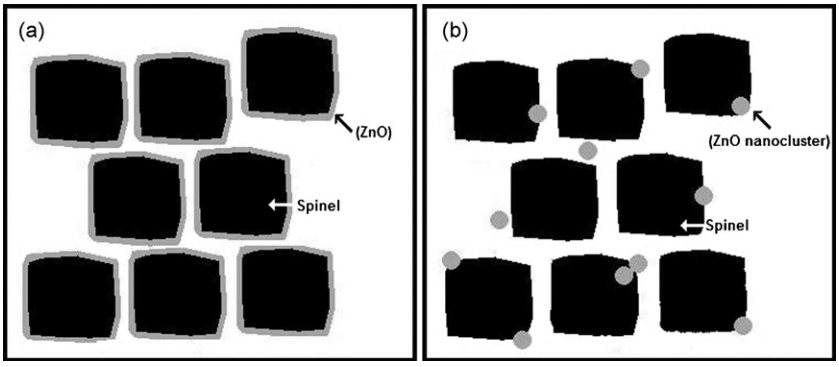

Fig. 4. Scheme for the ZnO deposition: (a) true coating and (b) nanoclusters uniformly dispersed in the bulk material.

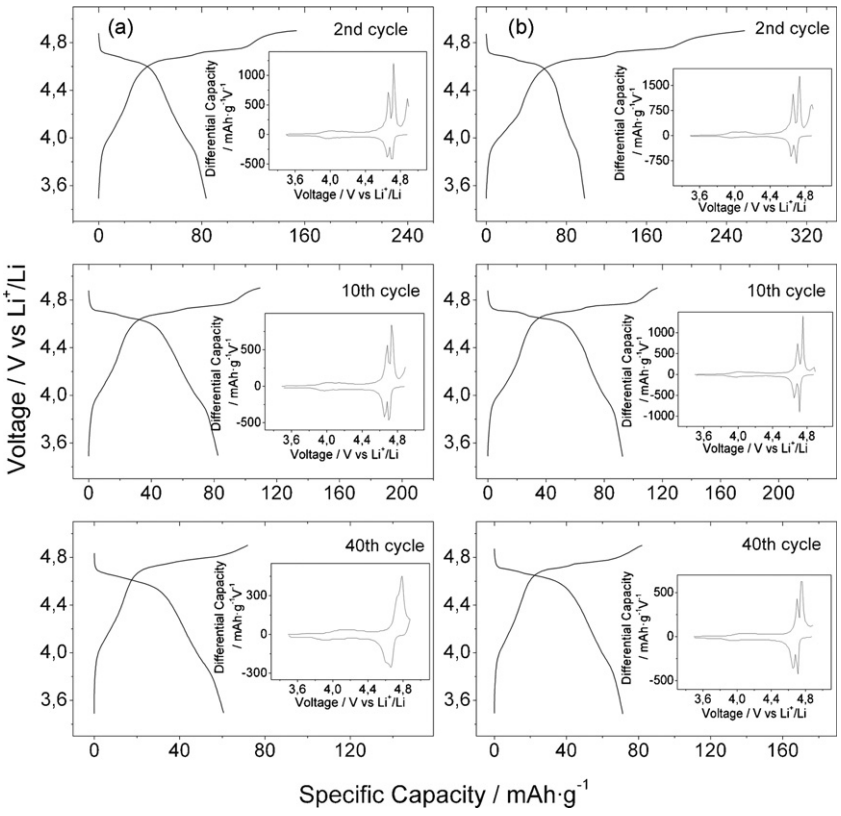

Fig. 5. Charge/discharge curves recorded at *C*/4 at 50 °C. The inset shows the corresponding capacity plots. (a) Pristine and (b) ZnO-treated spinel.

coating is deposited either as a chemical vapour (SiO_x [19]) or by sputtering (Au [12]). In these studies, the concentration of the element in the coating compound (Si, Au) was found to decrease in a quasi-hyperbolic manner with increasing sputtering time. This is consistent with coating of the pristine particles with a thin layer of the protective agent (see scheme in Fig. 4a).

As can be seen from Fig. 3b and the previous description, the Zn concentration varied differently with the sputtering time and suggests that the X-ray beam always "sees" a similar amount of Zn however long the sample is sputtered. Therefore, based on the depth profile data, the term "coating" is an inaccurate description for the ZnO-treated sample. The XPS results can be interpreted in the light of two different models. A reaction of ZnO with the spinel framework is rather unlikely since the changes in unit cell dimension, binding energies and full width at half maximum of the photoemission peaks for the spinel caused by the treatment with ZnO were all negligible. More likely, ZnO deposits as uniformly dispersed nanoclusters in the bulk material. This model is consistent with the EDAX image of Zn reported by Singhal et al. [16], where the spots, as with Ni, are evenly distributed. A scheme compatible with all these results is shown in Fig. 4b. We believe that this model can be extended to other systems (e.g. ZrO_2 [20], Al_2O_3 [21], MgO [22]) incorporated via a similar procedure where the formation of the precursor is followed by thermal treatment. Probably, these phases do not actually coat the active particles to be protected, but rather distribute uniformly in the bulk system. TEM images were consistent with this suggestion. In addition to the pseudo octahedral-like particles of the spinel, smaller particles (below 10 nm in size) randomly distributed were detected (see Fig. 2b). The fact that their appearance coincides with the treatment with the Zn salt gives a solid evidence to identify them as ZnO. Its low concentration and small particle size preclude its identification by XRD [13,16]. In any case, XPS depth profile analysis is the most accurate method to establish the actual nature of the additive.

3.2. Electrochemical properties

The electrochemical performance of the pristine and three ZnO-treated spinels was assessed from galvanostatic measurements made over a wide range of charge/discharge rates (*C*/4–8*C*) at cycling voltages from 3.5 to 4.9 V, both at ambient temperature and at 50 °C. Fig. 5a and b shows selected charge/discharge curves recorded at the latter temperature at *C*/4 in various cycles. For a better description of the different steps observed during Li removal and insertion, the figures include the differential capacity curves in an inset – pseudoplateaux have been converted into peaks for easier identification. As can be seen, the curves exhibit two regions of electrochemical activity, 3.9–4.4 V and 4.7–5.0 V. The former, characterized by a broad peak is related to the Mn^{3+}/Mn^{4+} redox couple and its very low in intensity is consistent with the presence of a very little Mn in the sample as confirmed by the stoichiometry given in Table 1. The recent assignation of the peaks at ca. 4.1 and 3.9 in the anodic and cathodic scans, respectively, to the Mn^{2+}/Mn^{3+} couple [16,23] can be ruled out on the basis of abundant reported evidence [2–9] and thermodynamic arguments [24]. Two well-defined peaks were obtained at high voltage that can be ascribed to the extraction and insertion of Li into the spinel framework. In redox terms, the removal of one Li atom per spinel formula involves the oxidation of Ni^{2+}–Ni^{4+}, the mechanism for which is thought to involve two cubic/cubic two-phase reactions [25]. Such reactions are highly reversible, as shown by the similar shape of the anodic and cathodic scans. The unresolved peak close to 4.9 V can probably be assigned to oxygen release from the spinel rather than to electrolyte decomposition [26]. In fact, it decreased upon cycling and was barely detectable in the 40th cycle.

The presence of ZnO had no significant effect on the shape of the galvanostatic curves (Fig. 5), which retained the strong signal assigned to the extraction and insertion of Li. However, splitting into two peaks was less clear. In fact, the two peaks in the cathodic

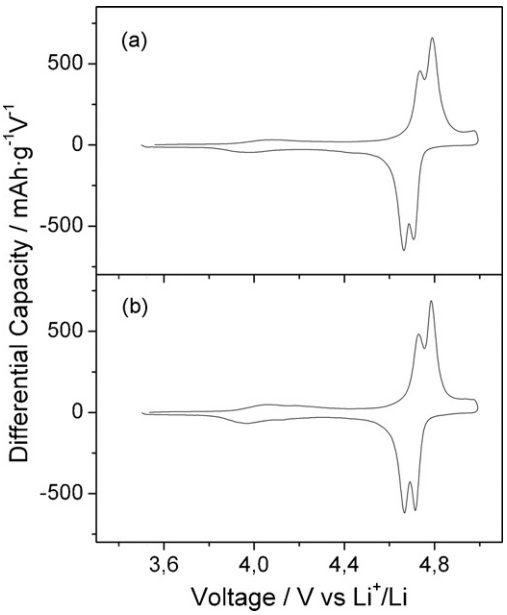

Fig. 6. Fortieth charge/discharge curves plotted as differential capacities recorded at 2*C* at ambient temperature. (a) Pristine and (b) ZnO-treated spinel.

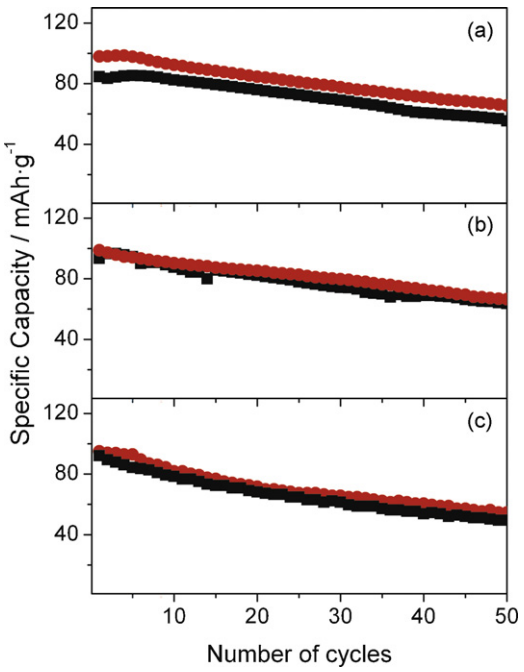

Fig. 8. Influence of the charge–discharge rate on the discharge capacity of Li/Li–Ni–Mn cells obtained from the original (black square) and ZnO-treated sample (red circle). Cycling tests were performed at 50 °C. (a) *C*/4, (b) 2*C* and (c) 4*C*.

and anodic scans overlapped into a broad, asymmetric signal for the untreated sample on prolonged cycling in measurements at a low rate (*C*/4, see Fig. 5a and b). This behavior is suggestive of a more sluggish kinetics of lithium transfer as a result of the protective effect of ZnO present. Moreover, the peak assigned to Mn^{3+} became weaker. At higher rates (above 2*C*), however, the presence of ZnO barely modified the shape profiles, not even on prolonged cycling (see Fig. 6). The two peaks at high voltages were well resolved, even when the spinel was treated with ZnO. All these features are relevant to the action of ZnO, which is more effective at low rates than it is at high rates; the effect, as shown below, is independent of the particular cycling temperature.

For easier understanding of the cell performance, we will first discuss the results obtained at room temperature. Fig. 7 shows the variation of the specific capacity with the number of cycles at 25 °C for the cells made from $LiNi_{0.5}Mn_{1.5}O_4$ and $LiNi_{0.5}Mn_{1.5}O_4$/ZnO. Four different rates (*C*/4, 2*C*, 4*C* and 8*C*) were selected to illustrate the cell behavior at intermediate rates. As can be seen, at low rates (*C*/4) the specific capacity delivered by the $LiNi_{0.5}Mn_{1.5}O_4$/ZnO spinel after the second cycle was higher than that of the cell made from $LiNi_{0.5}Mn_{1.5}O_4$. In this cycle, the capacity delivered by the bare spinel was 116 mAh g^{-1}, which is 12 mAh g^{-1} lower than that provided by the modified spinel (128 mAh g^{-1}). In the 50th cycle, the difference was not only maintained, but slightly increased to 14 mAh g^{-1}, which confirms the improved behavior

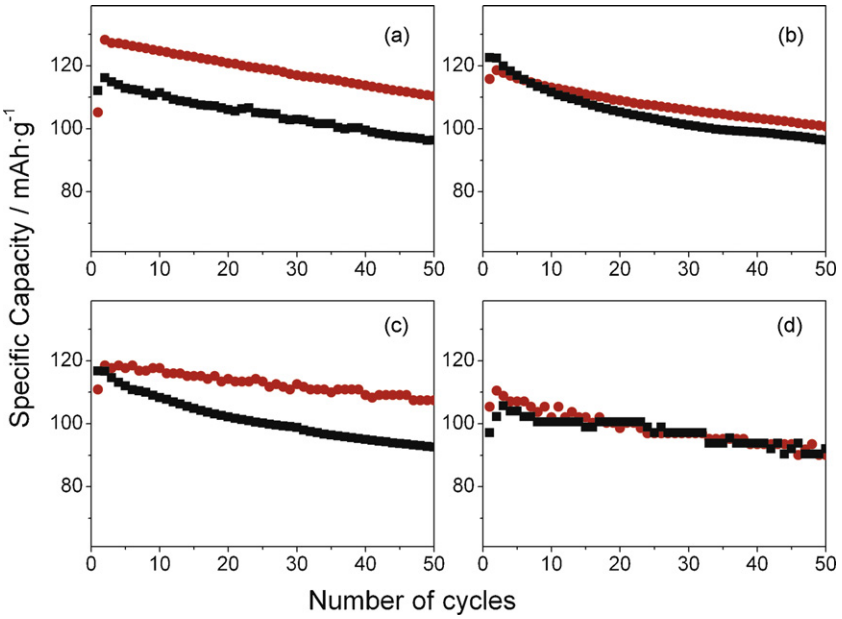

Fig. 7. Influence of the charge–discharge rate on the discharge capacity of Li/Li–Ni–Mn cells obtained from the original (black square) and ZnO-treated sample (red circle). Cycling tests were performed at room temperature. (a) *C*/4, (b) 2*C*, (c) 4*C* and (d) 8C.

Table 2
Coulombic efficiency (percent discharge/charge capacity ratio) obtained at *C*/4 and after a variable number of cycles.

Cycle	Room temperature (25 °C)		High temperature (50 °C)	
	$LiNi_{0.5}Mn_{1.5}O_4$	$LiNi_{0.5}Mn_{1.5}O_4$/ZnO	$LiNi_{0.5}Mn_{1.5}O_4$	$LiNi_{0.5}Mn_{1.5}O_4$/ZnO
2	63.2	57.4	54.3	58.9
10	87.8	96.8	75.4	81.5
30	90	97.5	81.2	87.7
50	90.8	96.9	84.2	88.6

of the $LiNi_{0.5}Mn_{1.5}O_4$/ZnO sample cycled at low rate. Other authors previously observed improved electrochemical performance of 4 V cathodic materials at low rates [27]. As confirmed below, ZnO protects the spinel nanoparticles from attack by hydrofluoric acid produced in the hydrolysis of the electrolyte salt by water traces. At low rates, where the nanosized material remains in contact with the electrolyte for a long time, ZnO acts as an efficient protector against acid reactivity. This hinders side reactions that degrade cell performance and results in an increased delivered capacity of the electrode relative to the untreated spinel. At 2*C* and 4*C*, the electrode made from the treated spinel also performed somewhat better than that obtained from the pristine spinel (see Fig. 7b and c). Thus, the delivered capacity of former electrode in the 50 cycle exceeded that of the latter by 8 mAh g^{-1} and 13 mAh g^{-1} at 2*C* and 4*C*, respectively. At 8*C*, both samples performed very similarly, the capacity tending to level off upon cycling (see Fig. 7d). The decreased protective efficiency of ZnO at high rates must be a result of the shorter time of contact between the active material and electrolyte (less than 8 min per step vs. 240 min at *C*/4). Based on these results, however, protection with ZnO is an interesting, simple method for improving the rate capability of the nanometric spinel $LiNi_{0.5}Mn_{1.5}O_4$. This treatment increases the specific capacity delivered by the spinel at low or moderate rates – where prolonged contact of the nanosized material with the electrolyte can boost side reactions through an increased reactivity and degrade cell performance as a result – without decreasing the discharge capacity at high rates (the greatest strength of nanosized materials in lithium cells).

The beneficial effect of ZnO was also observed at 50 °C, particularly at low rates. Fig. 8 shows the cycling properties of the cells at *C*/4, 2*C* and 4*C*. Under low charge/discharge regime, the initial specific capacity delivered by the pristine spinel was 84 mAh g^{-1}, which is more than 15% lower than that delivered by the modified spinel (98 mAh g^{-1}). Although the specific capacity of both cells faded upon cycling and capacity retention after 50 cycles was very similar (ca. 30 mAh g^{-1} was lost over 50 cycles), the electrode treated with ZnO retained the higher values. At higher rates, the effect of ZnO was less marked and both samples provided a similar electrochemical response. Sun et al. [13] previously found improved electrochemical properties in micrometric spinel $LiNi_{0.5}Mn_{1.5}O_4$, which they tested in this case at *C*/3 and 55 °C. These authors found that the electrode treated with ZnO (1.5 wt.%) virtually preserved the capacity (around 135 mAh g^{-1}) after 50 cycles. By contrast, the specific capacity of the uncoated electrode faded from 135 mAh g^{-1} at the first cycle to 45 mAh g^{-1} after 50 cycles. The improvement in our cells was not so dramatic, however. The origin of the difference is unclear since an electrode made from microparticles, as assessed elsewhere [28,29], should have exhibited acceptable performance (in between 120 mAh g^{-1} and 140 mAh g^{-1}) at this relatively low rate.

The beneficial effect of ZnO reached not only specific capacity, but also coulombic efficiency, defined as the discharge/capacity ratio (see Table 2). For simplicity, the table only lists the values obtained in a few cycles at *C*/4, where the effect of ZnO was especially marked. The coulombic efficiency was clearly increased by the presence of ZnO, the differences being somewhat smaller in the test carried out at 50 °C. Therefore, the presence of ZnO increases reversibility in lithium insertion/deinsertion – and the spinel stability under the cell operation conditions as a result.

Our results also rule out the possibility of ZnO hindering the formation of a graphitic phase by oxidation of the electrolyte as suggested by Sun et al. [15]. Had this been the case, the electrochemical performance of the electrode made from the untreated spinel would have been much worse than that observed in Figs. 5 and 6. The reaction of ZnO with HF traces coming from the electrolyte decomposition seems to provide a more realistic explanation for its beneficial effect. Removing HF must hinder dissolution of the spinel by attack of the acid. This explanation was indirectly substantiated by measuring the amount of HF released by standard titration [14]. Such an amount corresponded to HF evolved from the treatment of the original and coated spinel with 1 M $LiPF_6$ in 1:2 EC/DMC. However, the results obtained suggest that the presence of ZnO significantly reduces the release of HF, but provide no direct evidence for a direct attack of the acid on the spinel. Moreover, intrinsic errors associated to the gaseous nature of HF and its easy release from the liquid phase lead to spurious results. In fact, the significant differences in residual HF ratio for as-prepared $LiNi_{0.5}Mn_{1.5}O_4$ and 1.5% ZnO–$LiNi_{0.5}Mn_{1.5}O_4$ at 25 °C (37.5) and 50 °C (2.1) [14] require clarification as may have originated from these spurious effects of HF. We therefore used a direct method free of such shortcomings: to measure the reactivity of HF towards the spinel in the presence and absence of ZnO as determined from the amounts of Ni and Mn dissolved in each case. Such amounts are shown in Table 3 and warrant at least two comments. First, the Ni/Mn atomic ratio was quite similar in both samples and somewhat higher than that calculated from the spinel stoichiometry, 0.31 (see Table 1). This means that Ni is slightly easier to remove from the structure. Second and indeed significant, the amounts of Ni and Mn dissolved were smaller in the spinel treated with ZnO (26 and 19%, respectively). These results are quite consistent with a protective action of ZnO against the attack by HF.

Based on the above-discussed model for the location of ZnO nanoparticles, the spinel is also exposed to the electrolyte action and can react with HF released. We believe that this reaction is the main source of the capacity fading observed upon cycling in both the absence and presence of ZnO. However, ZnO can easily react by virtue of its amphotericity, so a portion of HF released is removed in this reaction. In fact, as shown by the ICP results, the presence of the oxide reduces the spinel solubility. The spinel can thus benefit from the increased tendency of HF to react with ZnO, thereby gaining stability under the cell operating conditions and delivering improved performance as a result – particularly at low rates.

Table 3
Amounts of Ni and Mn dissolved (ppm) after to treat the spinel with HF (sample weight 17 mg).

Sample	Ni	Mn	Ni/Mn[a]
$LiNi_{0.5}Mn_{1.5}O_4$	274.8	656.1	0.39
$LiNi_{0.5}Mn_{1.5}O_4$/ZnO	203.6	531.8	0.36

[a] Atomic ratio.

4. Conclusions

Treating nanosized $LiNi_{0.5}Mn_{1.5}O_4$ spinel with ZnO provides an effective method for enhancing its rate capability in lithium cells. This beneficial effect is more marked at low rates (*C*/4), where charge/discharge cycles and hence the interaction between the active material and electrolyte, lasts longer. At higher rates, the effect of ZnO was less marked and the pristine and treated samples provided a similar electrochemical response. The protective effect of ZnO was demonstrated by analysing the spinel solubility in aqueous HF. The presence of ZnO clearly reduced the spinel solubility in this medium, as reflected in the decreased amounts of Ni and Mn dissolved.

Acknowledgements

This work was performed with the financial support of the Ministerio de Educación y Ciencia (Projects MAT2008-03160 and MAT2005-03069) and Junta de Andalucía (Group FQM-175).

References

[1] P.G. Bruce, B. Scrosati, J.M. Tarascon, Angew. Chem. Int. Ed. Engl. 47 (2008) 1645 (and references therein).
[2] Q. Zhong, A. Bonakdarpour, M. Zhang, Y. Gao, J.R. Dahn, J. Electrochem. Soc. 144 (1997) 205.
[3] J.H. Kim, A.T. Myung, Y.K. Sun, Electrochim. Acta 49 (2004) 219.
[4] G. Armstrong, A.R. Armstrong, P.G. Bruce, P. Reale, B. Scrosati, Adv. Mater. 18 (2006) 2597.
[5] K. Ariyoshi, S. Yamamoto, T. Ohzuku, J. Power Sources 119–121 (2003) 959.
[6] Y.S. Lee, Y.K. Sun, S. Ota, T. Miyashita, M. Yosio, Electrochem. Commun. 4 (2002) 989.
[7] D. Kokacheva, H. Gadjov, K. Petrov, S. Mandal, M.G. Lazarraga, L. Pascual, J.M. Amarilla, R.M. Rojas, P. Herrero, J.M. Rojo, J. Mater. Chem. 12 (2002) 1184.
[8] J.C. Arrebola, A. Caballero, L. Hernán, J. Morales, E. Rodríguez Castellón, Adv. Funct. Mater. 16 (2006) 1904.
[9] Y. Talyosef, B. Markovsky, R. Lavi, G. Salitra, D. Aurbach, D. Kovacheva, M. Gorova, E. Zhecheva, R. Stoyanova, J. Electrochem. Soc. 154 (2007) A682.
[10] H. Yamane, T. Inoue, M. Fujita, M. Sano, J. Power Sources 99 (2001) 60.
[11] J.C. Arrebola, A. Caballero, L. Hernán, J. Morales, E. Rodríguez Castellón, Electrochem. Solid-State Lett. 8 (2005) A303.
[12] J.C. Arrebola, A. Caballero, L. Hernán, J. Morales, E. Rodríguez Castellón, J.R. Ramos Barrado, J. Electrochem. Soc. 154 (2007) A178.
[13] Y.K. Sun, Y.S. Lee, M. Yoshio, K. Amine, Electrochem. Solid-State Lett. 5 (2002) A99.
[14] Y.K. Sun, K.J. Hong, J. Prakash, K. Amine, Electrochem. Commun. 4 (2002) 344.
[15] Y.K. Sun, C.S. Yoon, I.H. Oh, Electrochim. Acta 48 (2003) 503.
[16] R. Singhal, M.S. Tomar, J.G. Burgos, R.S. Katiyar, J. Power Sources 183 (2008) 334.
[17] X. Liu, J. Wang, J. Zhang, S. Yang, Mater. Sci. Eng. A 430 (2006) 248.
[18] E. György, A. Perez del Pino, P. Serra, J.L. Morenza, Surf. Coat. Technol. 173 (2003) 265.
[19] H. Omanda, T. Brousse, C. Marhic, D.M. Schleich, J. Electrochem. Soc. 151 (2004) A922.
[20] D. Li, Y. Kato, K. Kobayakawa, H. Noguchi, Y. Sato, J. Power Sources 160 (2006) 1342.
[21] A.M. Kannan, A. Manthiram, Electrochem. Solid-State Lett. 5 (2002) A167.
[22] Z. Wang, C. Wu, L. Liu, F. Wu, L. Chen, X. Huang, J. Electrochem. Soc. 149 (2002) A466.
[23] R. Singhal, S.R. Das, O. Oviedo, M.S. Tomar, R.S. Katiyar, J. Power Sources 160 (2006) 651.
[24] J.M. Tarascon, D. Guyomard, J. Electrochem. Soc. 138 (1991) A2864.
[25] K. Ariyoshi, Y. Iwakoshi, N. Nakayama, T. Ohzuku, J. Electrochem. Soc. 151 (2004) 296.
[26] A. Caballero, M. Cruz, L. Hernán, M. Melero, J. Morales, E. Rodríguez Castellón, J. Electrochem. Soc. 152 (2005) A552.
[27] J. Tu, X.B. Zhao, J. Xie, G.S. Cao, D.G. Zhuang, T.J. Zhu, J.P. Tu, J. Alloys Compd. 432 (2007) 313.
[28] D. Aurbach, B. Markovsky, Y. Talyossef, G. Salitra, H.J. Kim, S. Choi, J. Power Sources 162 (2006) 780.
[29] J.C. Arrebola, A. Caballero, L. Hernán, J. Morales, J. Power Sources 180 (2008) 852.